ADVANCED MATERIALS
www.advmat.de

A Large-Scale Array of Ordered Graphene-Sandwiched Chambers for Quantitative Liquid-Phase Transmission Electron Microscopy

Kitaek Lim, Yuna Bae, Sungho Jeon, Kihwan Kim, Byung Hyo Kim, Joodeok Kim, Sungsu Kang, Taeyeong Heo, Jungwon Park, and Won Chul Lee**

Liquid-phase transmission electron microscopy (TEM) offers a real-time microscopic observation of the nanometer scale for understanding the underlying mechanisms of the growth, etching, and interactions of colloidal nanoparticles. Despite such unique capability and potential application in diverse fields of analytical chemistry, liquid-phase TEM studies rely on information obtained from the limited number of observed events. In this work, a novel liquid cell with a large-scale array of highly ordered nanochambers is constructed by sandwiching an anodic aluminum oxide membrane between graphene sheets. TEM analysis of colloidal gold nanoparticles dispersed in the liquid is conducted, employing the fabricated nanochamber array, to demonstrate the potential of the nanochamber array in quantitative liquid-phase TEM. The independent TEM observations in the multiple nanochambers confirm that the monomer attachment and coalescence processes universally govern the overall growth of nanoparticles, although individual nanoparticles follow different growth trajectories.

Liquid-phase transmission electron microscopy (TEM) avails an opportunity to study chemical reactions based on real-time and direct observations on a nanometer or sub-nanometer scale.[1] An observation of the reaction trajectories in liquid confirms previously suggested mechanisms and frequently reveals the importance of the processes that have been either underestimated or inadequately explored.[2] For example, liquid-phase TEM analyses of crystallization have demonstrated that non-classical pathways are heavily involved in the frame of the classical nucleation theory.[3] The kinetic and thermodynamic processes involved in the growth, etching, and interactions of colloidal nanoparticles have been successfully investigated on an atomic-scale resolution.[4,5] In those studies, a sealed nanoscale chamber (a liquid cell) encapsulated a thin liquid film between layers that were gas-impermeable, but electron-beam (e-beam)-transparent. The liquid cell facilitated the preservation of the liquid samples for in situ investigation in high-vacuum TEM.

The choices of suitable membrane materials that will improve the spatial resolution of the target systems in liquid-phase TEM have been explored. Compared to microfabricated thin films, such as SiN_x and Si (typically 30–100 nm thick, Figure S1a, Supporting Information),[6] utilizing graphene as the encapsulating layers of the liquid cell enables an atomic-scale observation of colloidal nanoparticles dispersed in a liquid (Figure S1b, Supporting Information).[7] The single-atom thickness, which is characteristic of graphene, minimizes the undesired e-beam scattering in TEM imaging. Additionally, sophisticated nanofabrication techniques, such as focused ion beam milling (FIB) and e-beam lithography (EBL) have been applied to the production of graphene liquid cells with precisely defined geometries.[8] Although such technical developments in liquid-phase TEM could enhance the unique capability of real-time observation, in situ investigations tend to rely on a limited number of exemplary occurrences observed by TEM. These occurrences hinder the understanding of the reaction mechanism in a quantitatively meaningful level. For example, a few observed trajectories of the growth of silver nanoparticles in a TEM field-of-view exhibited a diverse complexity of the types and growth rates.[9] Likewise, the differences in the local chemical conditions of a small volume of the encapsulated liquid sample can induce either the etching or growth of nanoparticles.[10] Such a diversity is ubiquitous in many chemical systems studied by liquid-phase TEM. Therefore, a new platform to acquire numerous in situ liquid-phase TEM data of the targeted chemical reaction is required. In this work, we develop an advanced liquid cell, equipped with a large-scale array of ordered graphene-sandwiched chambers, for quantitative data collection and demonstrate its application in the liquid-phase TEM analysis of colloidal nanoparticles.

K. Lim, Dr. S. Jeon, K. Kim, T. Heo, Prof. W. C. Lee
Department of Mechanical Engineering
Hanyang University
Ansan, Gyeonggi 15588, Republic of Korea
E-mail: wonchullee@hanyang.ac.kr

Y. Bae, Dr. B. H. Kim, J. Kim, S. Kang, Prof. J. Park
School of Chemical and Biological Engineering
and Institute of Chemical Processes
Seoul National University
Seoul 08826, Republic of Korea
E-mail: jungwonpark@snu.ac.kr

Y. Bae, Dr. B. H. Kim, J. Kim, S. Kang, Prof. J. Park
Center for Nanoparticle Research
Institute for Basic Science (IBS)
Seoul 08826, Republic of Korea

The ORCID identification number(s) for the author(s) of this article can be found under https://doi.org/10.1002/adma.202002889.

DOI: 10.1002/adma.202002889

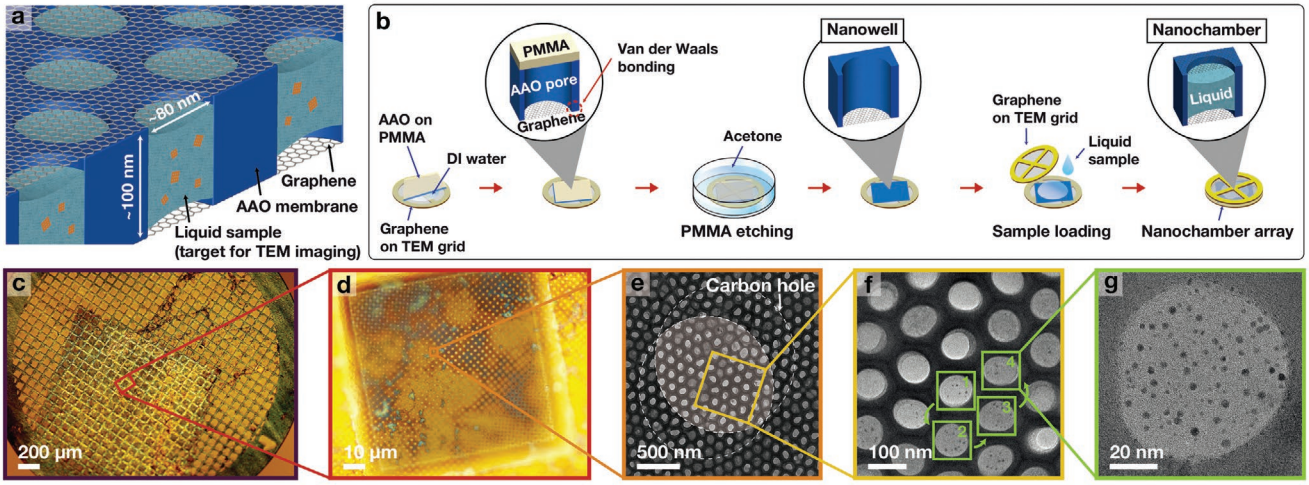

Figure 1. a,b) Schematics of the nanochamber array (a) and its fabrication process (b). c–g) Optical images and TEM images of the fabricated nanochamber array; c) a whole TEM grid, d) a single mesh, e,f) a nanochamber array, and g) a single nanochamber are shown.

The advanced liquid cell is fabricated by sandwiching a nanostructured membrane of anodic aluminum oxide (AAO) between layers of graphene (**Figure 1**a). The AAO membrane is filled with highly ordered uniform nanopores that are formed spontaneously and concurrently, during the anodization process, and the dimension of the nanopore is selectively controllable by changing the anodization parameters (Figure S2, Supporting Information).[11] In this work, we fabricate an exemplary design of the liquid cell, employing the AAO membrane with a pore diameter, interpore distance, and thickness of ≈80, ≈125, and ≈100 nm, respectively. The AAO membrane can afford ≈4.5×10^7 nanopores in a circular area with a diameter of 3 mm (typical size of a TEM grid). An individual nanopore, which is covered by the top and bottom graphene layers, forms an individual nanosized chamber (nanochamber), which can contain a liquid sample in a cylindrical inner space independently from each other. The number of constructed nanochambers is greater by several orders of magnitude than the scale achievable by successive nanopatterning of individual holes (FIB or EBL) used in the previous approaches,[8] allowing a collection of massive in situ data in a statistically meaningful level by repeating consecutive TEM observations throughout the large-scale array of the nanochambers.

The fabrication process of the liquid cell is illustrated in Figure 1b. Two graphene TEM grids, for the top and bottom layers of the liquid cell, are prepared by transferring graphene onto holey carbon TEM grids by direct transfer.[12] Deionized water is dropped onto the graphene-transferred grid. Thereafter the AAO membrane, supported on a poly(methyl methacrylate) (PMMA) substrate, is placed onto it. As the water is dried in an oven, the graphene layer and the AAO membrane are bonded by van der Waals force, which is strong enough to produce a hermetic seal that prevents leakage (first inset in Figure 1b).[13] The PMMA layer is thereafter, removed by immersing the assembled grid in an acetone bath. At that stage, nanosized-wells (nanowells) with an AAO sidewall and a bottom graphene layer (the second inset in Figure 1b) are formed. The fabricated nanowells with the bottom graphene layer are confirmed by TEM images and fast Fourier transform (FFT) patterns (Figure S3, Supporting Information). To load a liquid sample into the nanowells, the liquid sample is dispensed on the top of the AAO membrane, after which another graphene-transferred grid is placed onto it, thus encapsulating the liquid sample and bonding with the AAO membrane, simultaneously. The final structure is an array of cylindrical nanochambers, each of which consisted of a nanopore and top/bottom graphene layers with the encapsulated liquid sample (the third inset in Figure 1b). TEM imaging of the liquid sample is facilitated by passing e-beam through the graphene-sandwiched nanochambers. In this work, an aqueous precursor solution of chloroauric acid, octylamine, and cetyltrimethylammonium bromide is imaged to study the growth and diffusion of colloidal gold nanoparticles to demonstrate the application of the developed liquid cell in in situ TEM imaging.

The fabricated nanochamber array is observed at different magnifications to obtain an overview of the structures in a whole grid and in a single nanochamber (Figure 1c–g). The area on the TEM grid where AAO is transferred is distinct on the optical image (Figure 1c). Evenly distributed nanochambers with uniform diameters are observed and the identification of the nanochambers fully filled with the liquid samples is possible on TEM imaging at low magnification (Figure 1e,f; Figure S4, Supporting Information). Some of the nanochambers are empty or contain bubbles in encapsulated liquid, but the number of liquid-filled nanochambers is adequate for quantitative and repeated data collection. The thickness of the encapsulated liquid sample is estimated by using electron energy loss spectroscopy in cryo-scanning TEM measurement (Figure S5, Supporting Information). The averaged thickness over 20 nanochambers is 67.9 ± 26.8% of the depth defined by AAO membrane. Most nanoparticles (gray dots in Figure 1g) grow in the AAO hole (bright region), implying that the liquid samples in the different nanochambers are successfully separated. This further implies that the chemical condition inside a chamber is not affected by the observation in adjacent chambers. The process of repeating TEM imaging in multiple nanochambers is shown in Movie S1, Supporting Information, and Figure 1f. Because many nanochambers are regularly arranged and densely packed, it only requires a few seconds or minutes to move an area of observation from one chamber to another. It is also noteworthy that the AAO sidewall structures

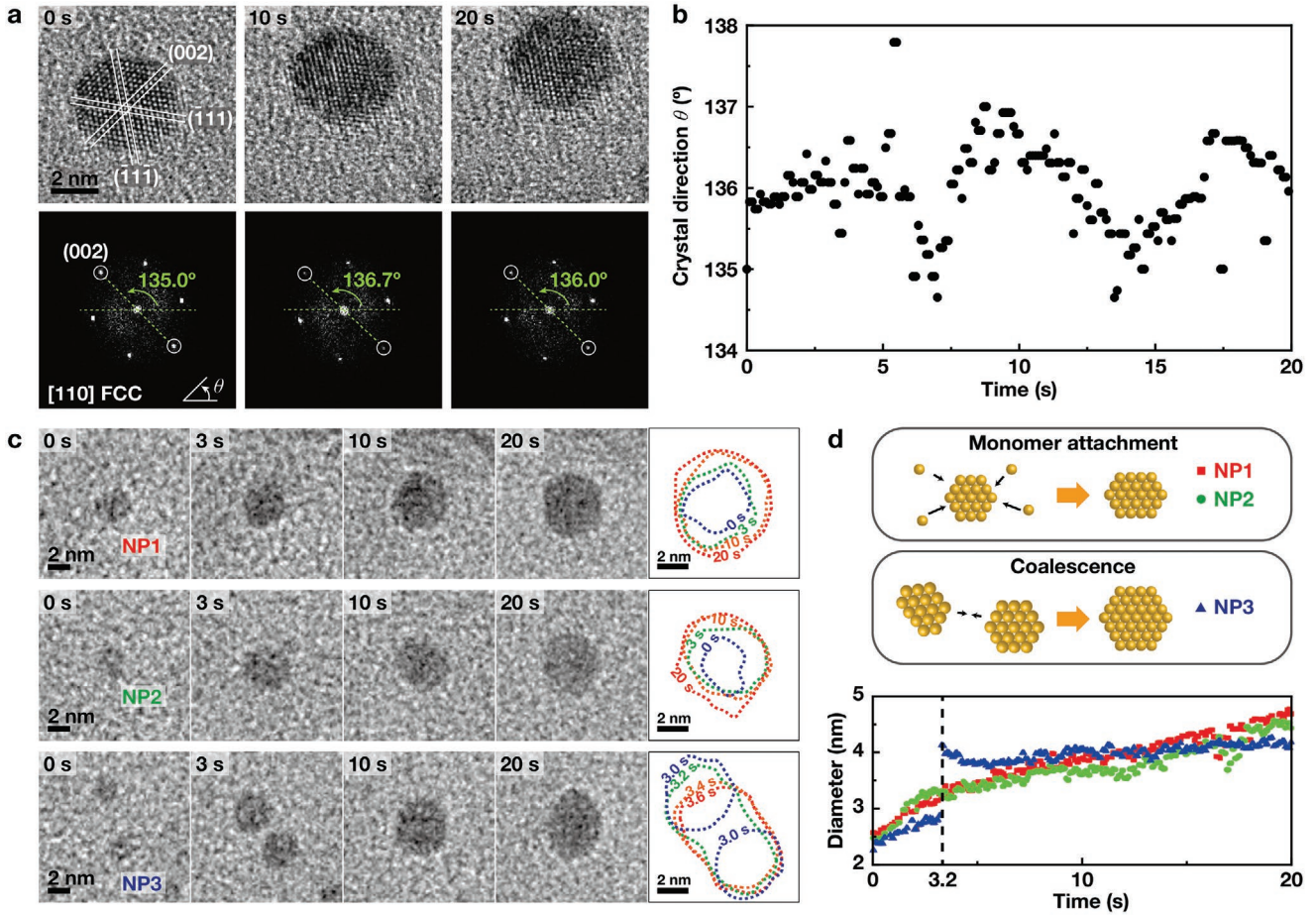

Figure 2. High-resolution TEM images and growth pathway of a gold nanoparticle in a nanochamber of the liquid cell. a) Snapshots from Movie S2, Supporting Information, and corresponding FFT patterns. b) Changes in the (002) crystal direction of the gold nanoparticle. c) Snapshot of TEM images from Movie S3, Supporting Information, and contour maps of the growing gold nanoparticles. d) Circular diameter trajectories for particles in (c).

in the nanochamber array affords an effective visual guide for coarse searching and focusing, during the sequential imaging processes of multiple chambers.

As previously noted, one of the major advantages of employing graphene is the enabling of high-resolution observation in liquid-phase TEM. A high-resolution TEM movie obtained with the fabricated nanochamber array, exhibiting a single gold nanoparticle with an initial diameter of 5 nm, is presented in Movie S2, Supporting Information. The atomic lattice fringes of the gold nanoparticle are clearly visible throughout a prolonged period, as shown in the TEM snapshots from Movie S2, Supporting Information and their corresponding FFT patterns (**Figure 2**a). A single crystalline face-centered-cubic (fcc) structure of the gold nanoparticle is identified by the measured lattice spacings and the angular differences between the bright spots for the (002), (–11–1), and (–111) planes in the FFT patterns. We also observe an in-plane rotational motion of the nanoparticle by monitoring the angular change of the FFT patterns. The orientation of the (002) peak is indicative of this rotational motion, which is plotted in Figure 2b. These results confirm that the developed liquid cell can achieve sub-nanometer spatial resolution in liquid-phase TEM.

We investigate the detailed pathways of the growth of the colloidal gold nanoparticles in a nanochamber by in situ TEM (Movie S3, Supporting Information). Three exemplary growth trajectories are captured in the liquid cell (Figure 2c,d). Initially, the three gold nanoparticles possess circular diameters of 2–3 nm. Noticeable increases in the diameters of the nanoparticle occur in the first 20 s, after which the growth slows down. The diameters of the two nanoparticles (NP1 and 2) increase continuously with time, indicating that the growth by monomer attachment[5,14] is dominant in the two cases throughout the period. Conversely, the growth of the third nanoparticle (NP3) involves a sudden increase in the diameter by ≈2 nm from 3 to 4 s. This sudden increase is due to the coalescence.[5,15] The detailed process of the coalescence, including neck formation, is presented in Figure S6, Supporting Information. The growth of the nanoparticle halts briefly just after coalescence in a process called the relaxation period.[5] Thereafter, the growth proceeds by monomer attachment. The above observations confirm that the growth of colloidal metal nanoparticles proceeds by two mechanisms: monomer attachment and particle coalescence, consistent with previous liquid-phase TEM investigations.[5,14,15]

The developed liquid cell affords repeated observations of nanoparticle growths and dynamics in multiple nanochambers in the same chemical conditions by carrying out consecutive imaging with the constant electron beam radiation.

Concentrations of radiolysis species in a given electron beam dose rate rapidly reach to the steady-state within 1 ms and maintain it thereafter (Figure S7, Supporting Information). The repeated observations facilitate numerous data collection. The independent observations of the generation and growth of gold nanoparticles in four different chambers of a liquid cell for 30 s are shown in the in situ movies (Movies S4–S7, Supporting Information). Enlarged TEM image frames extracted from the movies are shown in **Figure 3**a. The diffusion trajectories of the representative particles are indicated by a color gradient for time evolution from 0 (white) to 30 s (colored). The movement of the nanoparticles is analyzed by their mean square

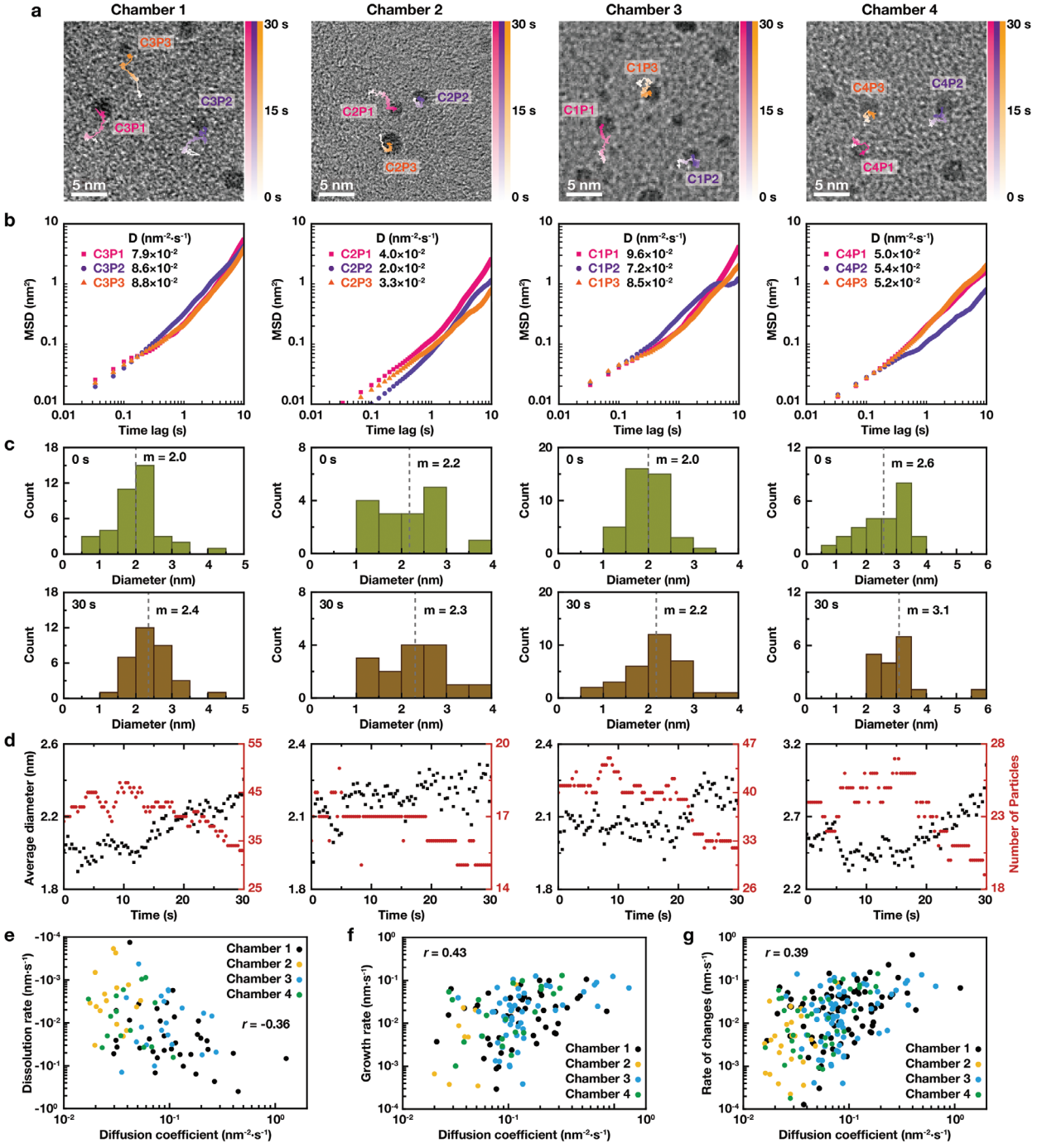

Figure 3. Growth and diffusion of the gold nanoparticles observed in four nanochambers of the liquid cell. a) Diffusion trajectories of three representative nanoparticles from four nanochambers. b) MSD as a function of time for 12 nanoparticles in (a). *D* is the diffusion coefficient. c) Histogram of the circular diameter of the nanoparticles in the four nanochambers at 0 and 30 s. The mean values are shown as dashed lines. d) Tracked average circular diameter and number of nanoparticles in the four nanochambers. e) Dissolution rate, f) growth rate, and g) rate of changes (absolute value of growth and dissolution rates) as a function of diffusion coefficients. *r* is the Pearson correlation coefficient.

displacement (MSD). The linearity expressed in the log–log plot of MSD indicates that the nanoparticles are dwelling in a fluid, following the Brownian motion.[16] The measured diffusion coefficient (D, in Figure 3b) is in the range of 1.9–9.6 × 10^{-2} nm^2 s^{-1} (Supporting Information).[1a,8a] Over the same period (0–30 s), the growth of the particles also occurs in each nanochamber. The distribution of diameters of the nanoparticles observed in each chamber can be measured at different periods of the growth, as shown in Figure 3c. The growth patterns observed in the different chambers are not identical. However, they share a similar general trend. The changes in the average size and the number of nanoparticles are tracked, as shown in Figure 3d. In the early stage (0 to ≈10 s), the average size of the nanoparticles slightly decreases because of the continuous generation of small clusters. Subsequently, the average size continuously increases to a level for a prolonged period. The number of particles decreases at this later stage, implying that coalescences are frequent as an alternative pathway in the growth. The observations obtained from multiple nanochambers reaffirm the involvement of coalescence along with monomer attachment, as important pathways in the growth of metal nanoparticles. The multi-chamber observations also reveal a positive correlation between diffusion coefficients and the rate of changes including dissolution and growth of individual nanoparticles (Figure 3e–g). The correlation is noticeably clear in a collective plot including all measurements from multiple chambers (Figure 3e–g), while it is unclear in a limited measurement from an individual nanochamber (Figures S8 and S9, Supporting Information), emphasizing the importance of the large-scale data collection from multi-chambers to correctly understand the behaviors of nanoparticles. The positive relationship implies that the surface reactions are highly correlated with the effective viscosity and relevant transport dynamics around the individual nanoparticles.

In this work, we developed a novel type of TEM liquid cell by sandwiching an AAO membrane between graphene layers. For the demonstration of its potential application in quantitative data acquisition and analysis, we performed TEM observations on colloidal gold nanoparticles dispersed in a liquid, with the fabricated nanochamber array. Our study confirmed that the diffusion dynamics and growth pathways of the colloidal nanoparticles can be studied in multiple chambers of a liquid cell while maintaining the high-resolution capability of graphene liquid-cell TEM.

Experimental Section

The detailed experimental process is available in the Supporting Information.

Supporting Information

Supporting Information is available from the Wiley Online Library or from the author.

Acknowledgements

K.L., Y.B., and S.J. contributed equally to this work. This work was mainly supported by the National Research Foundation of Korea (NRF) funded by the Ministry of Education (No. 2018R1D1A1B07050575 and 2019R1F1A1059099). S.J., K.K., and W.C.L. acknowledge the support from the convergence technology development program for bionic arm through the NRF, funded by the Ministry of Science & ICT (MSIT) (No. 2015M3C1B2052811). Y.B., B.H.K., J.K., S.K., and J.P. acknowledge the financial support from the Institute for Basic Science (IBS-R006-D1), the NRF grant funded by the Korean Government (MSIT) (Nos. NRF-2017R1A5A1015365 and NRF-2019M3E6A1064877), and Korea Toray Science Foundation. B.H.K. and J.P. acknowledge the support from the Samsung Science and Technology Foundation under Project number SSTF-BA1802-08 for method development, fabrication, and characterization.

Conflict of Interest

The authors declare no conflict of interest.

Keywords

anodic aluminum oxide, graphene liquid cells, in situ TEM, liquid-phase TEM

Received: April 28, 2020
Revised: June 28, 2020
Published online:

[1] a) F. M. Ross, *Liquid Cell Electron Microscopy*, Cambridge University Press, Cambridge, UK **2016**; b) F. M. Ross, *Science* **2015**, *350*, aaa9886; c) N. de Jonge, F. M. Ross, *Nat. Nanotechnol.* **2011**, *6*, 695; d) B. H. Kim, J. Yang, D. Lee, B. K. Choi, T. Hyeon, J. Park, *Adv. Mater.* **2018**, *30*, 1703316; e) H.-G. Liao, H. Zheng, *Annu. Rev. Phys. Chem.* **2016**, *67*, 719.

[2] a) C. Mueller, M. Harb, J. Dwyer, R. D. Miller, *J. Phys. Chem. Lett.* **2013**, *4*, 2339; b) M. Williamson, R. Tromp, P. Vereecken, R. Hull, F. Ross, *Nat. Mater.* **2003**, *2*, 532; c) W. C. Lee, B. H. Kim, S. Choi, S. Takeuchi, J. Park, *J. Phys. Chem. Lett.* **2017**, *8*, 647; d) G. Zhu, Y. Jiang, W. Huang, H. Zhang, F. Lin, C. Jin, *Chem. Commun.* **2013**, *49*, 10944; e) J. M. Yuk, Q. Zhou, J. Chang, P. Ercius, A. P. Alivisatos, A. Zettl, *ACS Nano* **2016**, *10*, 88; f) J. Wu, H. Shan, W. Chen, X. Gu, P. Tao, C. Song, W. Shang, T. Deng, *Adv. Mater.* **2016**, *28*, 9686; g) C. Yang, J. Han, P. Liu, C. Hou, G. Huang, T. Fujita, A. Hirata, M. Chen, *Adv. Mater.* **2017**, *29*, 1702752.

[3] a) M. H. Nielsen, S. Aloni, J. J. de Yoreo, *Science* **2014**, *345*, 1158; b) N. D. Loh, S. Sen, M. Bosman, S. F. Tan, J. Zhong, C. A. Nijhuis, P. Král, P. Matsudaira, U. Mirsaidov, *Nat. Chem.* **2017**, *9*, 77.

[4] a) Z. Liu, Z. Zhang, Z. Wang, B. Jin, D. Li, J. Tao, R. Tang, J. J. de Yoreo, *Proc. Natl. Acad. Sci. USA* **2020**, *117*, 3397; b) T. Su, Z. L. Wang, Z. Wang, *Small* **2019**, *15*, 1900050; c) C. Zhu, S. Liang, E. Song, Y. Zhou, W. Wang, F. Shan, Y. Shi, C. Hao, K. Yin, T. Zhang, J. Liu, H. Zheng, L. Sun, *Nat. Commun.* **2018**, *9*, 421; d) Z. Ou, Z. Wang, B. Luo, E. Luijten, Q. Chen, *Nat. Mater.* **2019**, *19*, 450; e) Z. Ou, B. Luo, C. Liu, Q. Chen, *Microsc. Microanal.* **2019**, *25*, 1414; f) J. M. Yuk, J. Park, P. Ercius, K. Kim, D. J. Hellebusch, M. F. Crommie, J. Y. Lee, A. Zettl, A. P. Alivisatos, *Science* **2012**, *336*, 61.

[5] H. Zheng, R. K. Smith, Y.-W. Jun, C. Kisielowski, U. Dahmen, A. P. Alivisatos, *Science* **2009**, *324*, 1309.

[6] a) M. J. Williamson, R. M. Tromp, P. M. Vereecken, R. Hull, F. M. Ross, *Nat. Mater.* **2003**, *2*, 532; b) C. Mueller, M. Harb, J. R. Dwyer, R. D. Miller, *J. Phys. Chem. Lett.* **2013**, *4*, 2339; c) J. M. Grogan, H. H. Bau, *J. Microelectromech. Syst.* **2010**, *19*, 885.

[7] a) M. Textor, N. de Jonge, *Nano Lett.* **2018**, *18*, 3313; b) J. M. Yuk, M. Jeong, S. Y. Kim, H. K. Seo, J. Kim, J. Y. Lee, *Chem. Commun.*

2013, *49*, 11479; c) J. Park, H. Park, P. Ercius, A. F. Pegoraro, C. Xu, J. W. Kim, S. H. Han, D. A. Weitz, *Nano Lett.* **2015**, *15*, 4737; d) C. Wang, T. Shokuhfar, R. F. Klie, *Adv. Mater.* **2016**, *28*, 7716; e) K. H. Nagamanasa, H. Wang, S. Granick, *Adv. Mater.* **2017**, *29*, 1703555.

[8] a) D. J. Kelly, M. Zhou, N. Clark, M. J. Hamer, E. A. Lewis, A. M. Rakowski, S. J. Haigh, R. V. Gorbachev, *Nano Lett.* **2018**, *18*, 1168; b) H. Rasool, G. Dunn, A. Fathalizadeh, A. Zettl, *Phys. Status Solidi* **2016**, *253*, 2351.

[9] T.-Y. Ahn, S.-P. Hong, S.-I. Kim, Y.-W. Kim, *RSC Adv.* **2015**, *5*, 82342.

[10] K. W. Noh, Y. Liu, L. Sun, S. J. Dillon, *Ultramicroscopy* **2012**, *116*, 34.

[11] W. Lee, S.-J. Park, *Chem. Rev.* **2014**, *114*, 7487.

[12] W. Regan, N. Alem, B. Alemán, B. Geng, Ç. Girit, L. Maserati, F. Wang, M. Crommie, A. Zettl, *Appl. Phys. Lett.* **2010**, *96*, 113102.

[13] S. P. Koenig, N. G. Boddeti, M. L. Dunn, J. S. Bunch, *Nat. Nanotechnol.* **2011**, *6*, 543.

[14] M. Jeong, J. M. Yuk, J. Y. Lee, *Chem. Mater.* **2015**, *27*, 3200.

[15] a) K.-Y. Niu, H.-G. Liao, H. Zheng, *Microsc. Microanal.* **2014**, *20*, 416; b) F. Wang, V. N. Richards, S. P. Shields, W. E. Buhro, *Chem. Mater.* **2014**, *26*, 5.

[16] X. Michalet, *Phys. Rev. E* **2010**, *82*, 041914.